ADVANCED FUNCTIONAL MATERIALS
www.afm-journal.de

Maintaining Cytocompatibility of Biopolymers Through a Graphene Layer for Electrical Stimulation of Nerve Cells

*Peter C. Sherrell, Brianna C. Thompson, Jonathan K. Wassei, Amy A. Gelmi, Michael J. Higgins, Richard B. Kaner, and Gordon G. Wallace**

Here, the utility of large-area graphene as a flexible, biocompatible electrode to stimulate cell growth is demonstrated. Chemical vapor deposition allows the production of highly crystalline, single, double, or few-layered graphene on copper substrates. The subsequent transfer to a biopolymer support, such as polylactic acid (PLA) or polylactic-co-glycolic acid (PLGA) copolymers, provides a unique electrode structure retaining the flexibility and surface properties of the underlying materials with a conductive graphene layer sufficient to enable electrical communication with excitable cells. The growth and compatibility of PC-12 cells on these graphene-biopolymer (GPB) electrodes is influenced more by the underlying polymer than the presence of graphene, demonstrating that the characteristics influencing biocompatibility have been retained after graphene modification. Differentiation of these cells into neural phenotypes is enhanced using electrical stimulation through the graphene conductive layer, confirming that the conductivity of graphene is sufficient to electrically communicate with cells grown on the surface. The process described herein demonstrates that non-conducting, flexible biopolymer surfaces can be easily coated with graphene without changing the biocompatibility of the materials. This could be used to create electrodes from non-conducting materials with optimized cell compatibility with graphene providing electrical properties suitable for stimulation of cells without greatly changing the surface properties.

1. Introduction

One of the key challenges in medical bionics is to interface, stimulate and regenerate the human neural system. Enhancing the communication between electrodes and the neural system will have immediate impact on existing medical bionics devices such as the cochlear implant, an artificial retina implant, vagus nerve stimulators (for controlling epilepsy and pain management) and deep brain stimulators for the control of Parkinson's disease. More effective communication could also enable the development of other applications such as nerve regeneration or effective neural connections to wearable prosthetics.[1] Here, we describe a process to modify non-conducting, degradable, biocompatible polymers with graphene to create an electrode capable of electrical communication with cells resulting in a flexible and biocompatible composite electrode.

Each of the aforementioned implants require the development of novel structures and configurations that induce the formation of an effective electrode–cellular interface.[2] This also means that the electrode structure must be cytocompatible and have sufficient flexibility and mechanical properties to be handled throughout surgery, and to cope with movement of the surrounding tissues in the body.

Typically, fabrication of such materials is a significant challenge since conductive materials are generally mechanically rigid. The difference between the modulus of the conductive material and the surrounding tissue can be problematic, both in terms of communication between the conductor and nerve cells, and the tissue response in the vicinity of the implanted material. Recent interest in developing soft, pliable, conductive materials has led to heightened research into the use of organic conductors.[1] Flexible, conducting materials have previously been described, notably in the work of Gross et al. on CNT flexible conductive electrodes for neural recordings[3] and Rogers et al. on flexible silicon electronics on biocompatible silk,[4] however the conductivity and mechanical properties are intertwined and not independently variable.

One material with the potential to provide conductive layers on flexible substrates is graphene.[5] Chemical vapor deposition can produce both single and bilayers of sp^2 hybridized graphene on metal catalysts. One crucial advantage of this growth method is the ability to grow and transfer large-area graphene onto a range of different substrates, using metal etching to leave the graphene adhered to another mechanically supporting material.[6–14] Traditionally, this transfer has been

Dr. P. C. Sherrell, Dr. B. C. Thompson, A. A Gelmi, Dr. M. J. Higgins, Prof. G. G. Wallace
ARC Centre of Excellence for Electromaterials Science
Intelligent Polymer Research Institute
AIIM Facility, Innovation Campus
University of Wollongong
NSW 2522, Australia
E-mail: gwallace@uow.edu.au
Dr. J. K. Wassei, Prof. R. B. Kaner
Department of Chemistry & Biochemistry and
California NanoSystems Institute
University of California
Los Angeles, CA, 90095, USA

DOI: 10.1002/adfm.201301760

achieved through the spin-casting of thin layers of poly(methyl methacrylate) (PMMA) onto graphene-coated copper foil followed by etching of the copper by concentrated HCl and $FeCl_3$. The etching process produces graphene on PMMA, which is then cleaned and deposited onto a range of substrates followed by polymer dissolution. Here we present an abridged process in which graphene is simply transferred onto a range of PLA and PLGA bio-polymers, a flexible and biocompatible substrate, via solution casting or melt processing methods, followed by the removal of copper.

CVD graphene is mechanically robust, opening unique avenues to design conductive, flexible and biocompatible electrodes with a controllable modulus. It has been found that varying the number of graphene layers allows the formation of tunable band-gaps in bilayer graphene over small areas.[15–17] In all cases regarding synthesis, there has been a significant focus on the lattice overlay structure (ABAB vs ABC), which is poorly controlled over large areas. The interest in bilayer graphene for this application, however, is not the tunable band gap property, but rather the conductivity, chemical stability and mechanical support that other materials do not provide. Specifically, the utilization of bilayer graphene allows an increased conductive pathway over rough, flexible substrates. It is hypothesized that bilayer graphene could conform tightly to the polymer layer while remaining electrically conductive as a continuous layer over large vertical height step changes. The basis of this hypothesis is that it is well known that elastomeric polymers will make conformal contact with surfaces and that graphene is able to withstand considerable amounts of strain. As such these two materials are able to adhere to each other and withstand flexion. This is supported by high impedance multimeter 2 point probe analysis of the materials showing that there was a conductive path over the entirety of the 2 cm × 3 cm graphene-on-polymer constructs used for this study, with resistance from edge to edge measured in the magnitude of 10 kΩ. Many points (30 or more, chosen at random across the 2 cm × 3 cm electrode surfaces) were measured over at least 5–6 electrodes produced in the same way, with no recording ever showing a lack of continuity, confirming that the conductive pathways were seen quite consistently over the surfaces.

Polylactic acid (PLA) and polylactic-co-glycolic acid (PLGA) are biocompatible and biodegradable synthetic polymers made from polymerization of lactic acid and glycolic acid. PLGA materials, in particular, have found many applications in several biomedical devices, starting from their use as bio-resorbable sutures in the 1970s and moving towards more nanotechnological applications in recent years.[18] Increasing the proportion of glycolide relative to lactide in the polymerization leads to softer films that have higher rates of degradation.[19,20] PLA and PLGA films were chosen for this study due to the ability to tailor the mechanical properties within the same family, and for the known biocompatibility of these materials. It is known that varying the softness of the underlying materials changes the way that nerve cells grow and differentiate in culture,[21] as too would be expected from PLA and PLGA materials with different mechanical properties. Recently, it has been shown that CVD graphene sheets can mimic the surface chemistry of the underlying substrate.[22] This in principle should mean that the nerve (PC-12) cells used in this study should respond more to the surface and mechanical properties of the different PLGA formulations than to the presence of the graphene. The implication of this would be that graphene can be used to provide a conducting layer on materials with good biocompatibility, without changing the properties influencing the cell response to the material.

Here, we explore the transfer of CVD-grown bilayer graphene onto a range PLA and PLGA blends. We demonstrate that the rate of nerve cell growth is based on the properties of the underlying PLGA, and not graphene modification. We then provide the first report of electrical stimulation of cells on graphene to enhance the differentiation into a neural phenotype. These results show that the process of transferring graphene onto non-conducting biocompatible polymers can be used to create a flexible electrode that is sufficiently conductive for electrical communication with cells while retaining the cytocompatibility of the base polymer.

2. Results and Discussion

2.1. Synthesis and Physical Characterization

Variations in the CVD growth conditions, such as partial pressure, flow rate and temperature afford the growth of either 1 or 2 layers of graphene on the copper substrate. Optical imaging reveals the presence of multi-layer graphene (**Figure 1**a) and those areas on the copper where there is only single-layer graphene. (Figure 1b). Raman spectroscopy confirms these regions as single, multi-, or few layered graphene based on the 2D:G ratio and the full width at half maximum (FWHM) of the 2D peak (**Figure 2**a). The graphene was then transferred onto a range of PLA and PLGA biocompatible polymer films (PLA, which is equivalent to 100:0 PLGA, 75:25 PLGA, and 50:50 PLGA) through drop-casting the pre-cured polymer over areas up to 9 cm^2, forming graphene-biopolymer composites (GBP). After a brief curing process, the copper was etched away utilizing a $HCl/FeCl_3$ etchant solution (Sigma-Aldrich). Prior to etching, the uncoated side of the copper film was cleaned vigorously to remove any graphene layers from the surface. Atomic force microscopy (AFM) imaging of the PLA:PLGA and GBP showed that the graphene generally follows the underlying topography of the polymers, including the undulating changes in height over the scan area and voids in the surface (Figure 1c). At higher magnification, however, the graphene contributes to smaller variations in height (secondary roughness) that appear to arise due to wrinkling of the graphene. Root mean squared (r.m.s.) roughness values varied significantly due the undulating height changes and voids of the different polymer films, with r.m.s. roughness values ranging between ≈30–150 nm (over the entire scan area). The sampling and extent of these micron scale topographic features were dependent on the scan location, thus making a direct comparison of the r.m.s. roughness between polymers difficult. However, their elimination by way of masking the area for the roughness analysis (e.g., removing primary roughness or waviness) showed that the secondary roughness of the polymers were relatively comparable with values of 25–50 nm (over a 5 μm^2 area). After transfer of

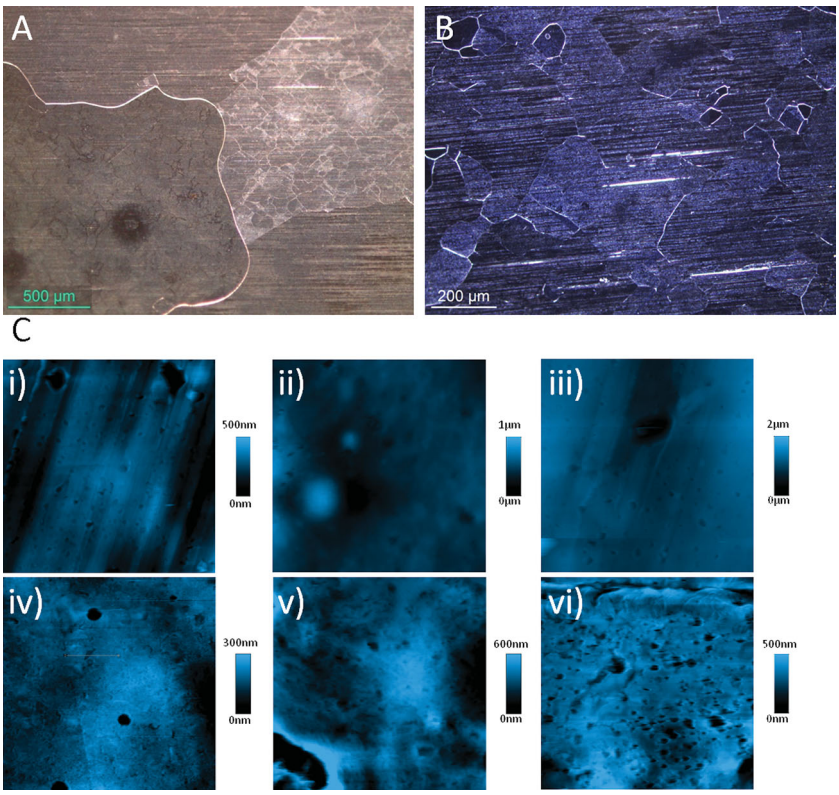

Figure 1. Optical images of carbon deposits on copper foils after the thermal decomposition of methane; a) Single, few and multi-layered graphene sheets; b) single layer graphene sheets. c) 20 µm by 20 µm atomic force microscopy images detailing the surface topography of graphene–polymer composite films in phosphate buffered saline solution. The pristine polymers are i) 50:50 PLGA; ii) 75:25 PLGA; iii) PLA. The graphene composite (GBP) forms are iv) 50:50 PLGA; v) 75:25 PLGA; vi) PLA.

the graphene, a similar range of 20–45 nm (over a 5 µm^2 area) indicated that the secondary roughness component did not significantly change.

2.1.1. Raman Spectroscopy and Analysis

Raman spectral analysis of the GBPs shows both the graphitic G band at ≈1580 cm^{-1} and the 2D band ≈2650 cm^{-1}, confirming the successful transfer of graphene (Figure 2b). Due to signal damping from the soft polymer layer, quantitative analysis of the number of transferred layers is not possible; however, qualitatively (from the Raman mapping of graphene on copper, not shown) it can be stated that predominantly bilayer graphene was transferred onto the polymer structures. Crucial to the confirmation of the successful transfer of bilayer graphene onto the polymers is the analysis of the full width at half maximum (FWHM) of the 2D peak subsequent to this transfer.[23–26] To this end, high resolution Raman spectroscopy with an 1800 line mm^{-1} grating was utilized; analysis of the as-grown graphene on copper shows four distinct peaks at 2636 cm^{-1}, 2643 cm^{-1}, 2671 cm^{-1}, and 2687 cm^{-1}, respectively (Figure 2c). Transfer of the graphene onto the bio-polymers results in a red shift of these peaks to 2641 cm^{-1}, 2648 cm^{-1}, 2664 cm^{-1}, and 2679 cm^{-1}, respectively, with a corresponding decrease in relative intensity of the peaks at higher wavenumbers (Figure 2d). This decrease in peak intensity arises due to the interaction of the graphene with the polymer substrate causing a change in the way the layers vibrate with respect to each other. Such a change in vibrational mode is analogous to the restriction of the radial breathing modes of single-walled carbon nanotubes with the presence of polymers or surfactants.[27–29] Alternatively, this decrease could also arise from doping of the graphene by the underlying polymer, highlighting the difficulties in quantitative Raman spectroscopic analysis of graphene composites.

2.1.2. Goniometry

Surface wettability is of paramount importance for cytocompatibility. To understand the changes in the surface energies of the GBP structures, room-temperature goniometric measurements were performed using 200 µL droplets of distilled water. PLA films were measured to have a contact angle of 68 ± 12° and the addition of graphene caused the contact angle to increase to 75 ± 7°, indicating only a slight change in the wettability of the material. This change arises either due to the addition of a hydrophobic surface to the material, or an increased nanoscale roughness after coating. Interestingly, there was a dramatic increase in hydrophilicity when PLGA was utilized, with the resultant contact angle approaching 0° and being immeasurable for both etched PLGA and PLGA GBPs. This finding that the wetting properties of the graphene surface approach that of a super-hydrophilic surface is contrary to its expected hydrophobic character and thus provides further evidence that the graphene is in fact mimicking the surface properties (i.e., high surface energy) of the underlying PLGA.

2.1.3. Electronic Properties

The focus of this paper is to demonstrate the stimulation of nerve cells on graphene sheets. To determine the conductivity of the material after graphene transfer, sheet resistance values were measured using both a high impedance multimeter and a linear 4-point probe system. The resistance of these films was observed to vary greatly depending on the contact area of the dried film with the graphene substrate. Typical values of resistance were 10 kΩ over a linear 3 cm distance, measured using a high impedance multimeter. Utilizing a linear 4-point probe geometry, the sheet resistance of the GBP films was determined. The measured resistivities of the GBP samples were all around 1 kΩ cm^{-1}, with PLA GBP at 1000 ± 500 Ω cm^{-1}, 75:25 GBP at 900 ± 200 Ω cm^{-1} and 50:50 GBP at 1400 ± 800 Ω cm^{-1}. There was a large variation within all of the examined samples, which can be attributed to poor contact between the probes and the sample as well as small imperfections in the

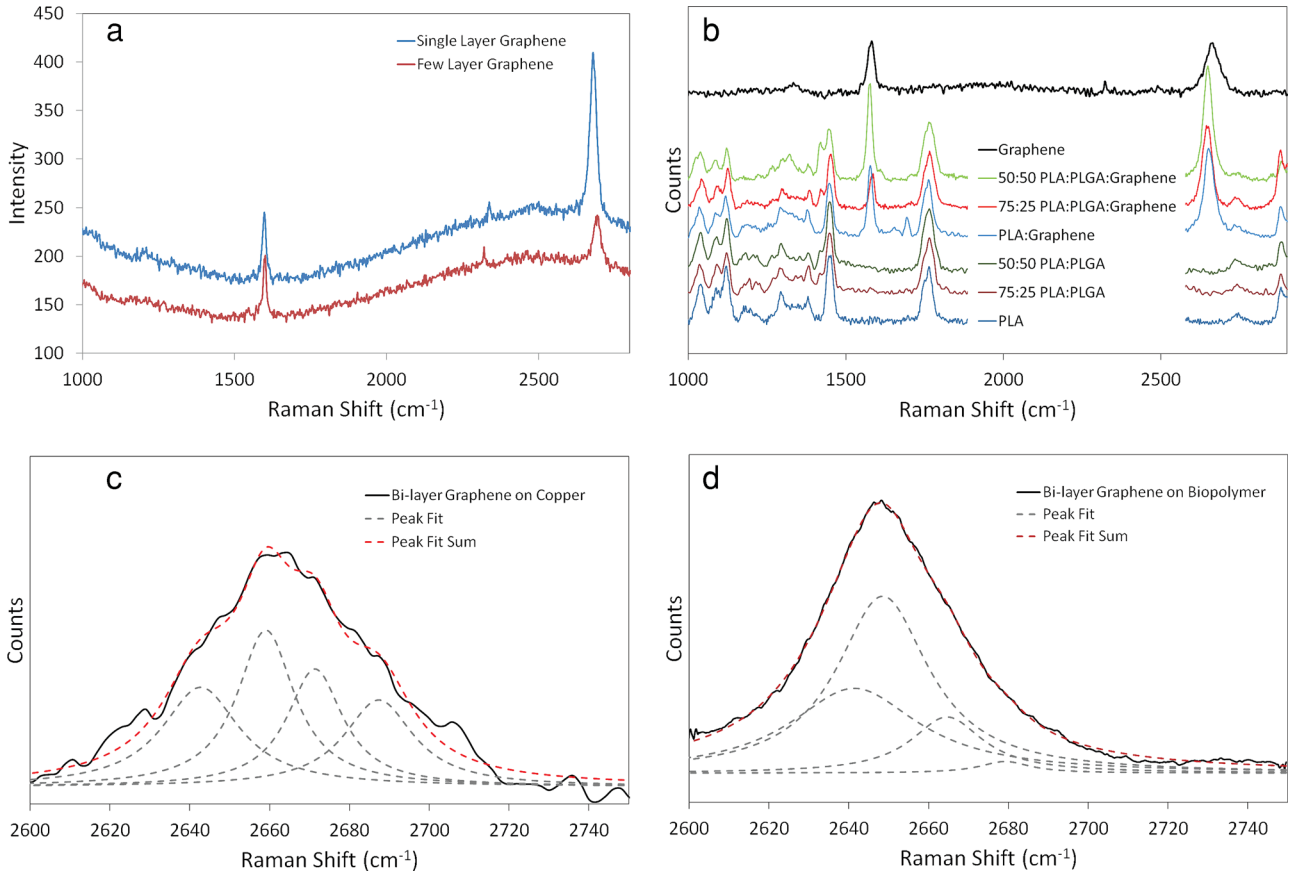

Figure 2. Raman spectra and analysis of graphene used for the cell stimulation studies. a) Raman spectra of graphene on copper sheets showing the difference in 2D band excitation between regions of single layer and few-layer graphene; b) Raman spectra of biopolymer composites with and without transferred graphene. Raman spectral fits of the 2D band c) bilayer graphene on copper; and d) bilayer graphene on PLA.

graphene over the 3 cm distance. This poor contact is a function of both the soft polymer in relation to the significantly stiffer probe and the approximately 1 nm thickness of the conductive layer. The relatively low resistivity of the GBP composites demonstrates the utility of graphene as a viable electrode material, which is shown later for the electrical stimulation of nerve cells.

A 1 cm^2 (geometric surface area) 50:50 GBP electrode was placed into a bath of 1 m $NaNO_3$. Using cyclic voltammetry (scan rate of 0.05 V s^{-1}), specific capacitance values were determined to be of the order of 7 μF cm^{-2} (Figure S-1, Supporting Information). This value is near the lower boundary of charge for a Helmholtz double layer capacitance with a 1 cm^2 electro-active surface area, expected to be between 5 and 20 μF cm^{-2}.[30–32] We attribute the measured capacitance value to three possible reasons. First, the range of expected capacitance values were measured using bulk carbon materials with resistivities of 10 to 100 Ω cm^{-1}, while these GPB structures use graphene with a resistivity of ≈1000 Ω cm^{-1}. Second, there is a significant signal loss when making contact to these GBP structures due to contact resistance. Third, the capacitive response can be affected by the step-height changes in the polymer that can induce stress in the graphene and increase resistance in those areas.

2.1.4. Mechanical Properties

To understand the mechanical properties of these GBP composites under compressive forces in physiologically relevant conditions, AFM force measurements were collected using a silicon nitride tip with a spring constant of 20 N m^{-2} and maximum applied load of 40 nN in phosphate buffered saline. For these measurements, force mapping was performed by taking a 32 × 32 array of force curves in order to sample the material properties across the GBP surface (**Figure 3**). The force maps display the slope (N.m^{-1}) of the tip-sample contact region with their color scale from 0 to 10 N.m^{-1} indicating the stiffness of the material (i.e., lighter areas are stiffer). The AFM maps were able to show a general trend in the stiffness of the polymers and, importantly, indicate any changes after transfer of the graphene. The stiffness of the pristine polymers decreased in the order of 50:50 PLGA ≈ 75:25 PLGA > PLA (Figure 3a, i–iii). Compared to the other polymers, the PLA consisted of nanoscale lateral variations in the stiffness with regions of low stiffness (dark areas) significantly contributing to the overall stiffness of these polymers (Figure 3a, iii). After transfer of the graphene, the above trend in the stiffness did not change for the corresponding GBP polymers (Figure 3b, i–iii). The PLA (GBP) again showed the greatest lateral variation in stiffness

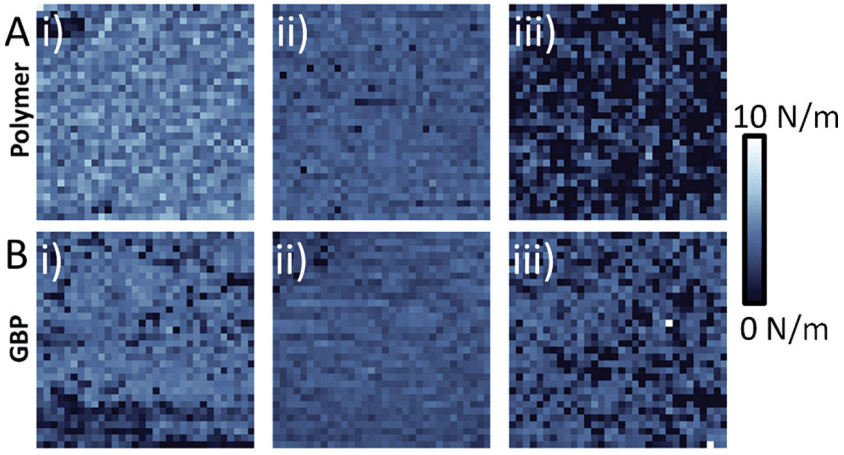

Figure 3. Atomic force microscopy force maps (32 × 32 force curves) taken over a 20 µm by 20 µm area of the polymers in phosphate buffered saline solution. The data (each pixel) represent the slope (N/m) of the contact region in the force curves or effective stiffness of the interaction with the polymer. The force maps for the pristine polymers A) are i) 50:50 PLGA; ii) 75:25 PLGA; iii) PLA and for their GBP forms B) are i) 50:50 PLGA; ii) 75:25 PLGA; iii) PLA.

across the surface, even though this effect slightly diminished for PLA (GBP) (Figure 3b, iii) and appeared for 50:50 PLGA (GBP) (Figure 3b, i). Importantly, the magnitude of the stiffness for the GBP composites did not significantly change within the measured variation, indicating that the addition of the graphene layer did not significantly increase the stiffness, as one might have expected for these high modulus materials. Thus, the graphene did not impact on the surface mechanical properties with the observed stiffness correlated to that of the underlying polymers.

2.2. Cell Interactions

2.2.1. Cell Growth and Differentiation Studies

In order to assess the suitability of these composite materials before the application of electrical stimuli to cells, the adhesion and proliferation of a rat neural model cell line (PC-12) was first assessed using a Pico Green assay. This assay estimates the cell density by measuring the amount of DNA in solution after lysing the cells. As shown in **Figure 4**, at 24 h after seeding, there was no difference in the adhesion and early proliferation of the PC-12 cells on any of the materials. However, the cell density on 50:50 PLGA, or 50:50 GBP had started to increase over other materials at 48 h. This increased proliferation rate continued on to 4 days, with a significantly increased cell density on both the coated and uncoated materials. After a longer lag phase, PC-12 proliferation also increased on the 75:25 PLGA biopolymer at 96 hours, and again, the cell growth observed was similar for GBP and unmodified PLGA. Cell proliferation was minimal on PLA, with only a slight increase in cell number after 24 h. The cells were observed to be over 97% viable by live/dead analysis (data not shown) on all materials, with no differences in cell viability observed between samples. Based on these results, the 50:50 PLGA material provided the optimal biopolymer formulation and was then used to make the GBP structures to study the efficacy of stimulated cell growth.

2.2.1. Electrical Stimulation of PC-12 Nerve Cells

PC-12 cells differentiate into a neural phenotype when exposed to protein nerve growth factor, and this property has led to their widespread use as a model for neural differentiation. The degree of differentiation, as measured by the length of neurites expressed by the differentiating cells, is known to be enhanced with electrical stimulation, again providing a model of electrical stimulation-induced increase in nerve differentiation.[33–35] Cells were seeded onto the GBP structures at a density of 2000 cells cm^{-2} in 4 well chamber slides (area ≈ 1.5 cm^2), and changed to differentiation media after approximately 14 h. Electrical stimulation was applied for 8 h per day for 3 days, and the cells were fixed and stained immediately after the last period of electrical stimulation. The voltage output for this current controlled stimulation is shown in Figure S-2 (Supporting Information), and was consistent over the 3-day testing period. As shown in **Figure 5**, the effect of electrical stimulation on the PC-12 cells was dramatic, with a large increase in the neurite length and connectivity of the neurites (Figure 5b) compared to unstimulated cells (Figure 5a). This indicates an increase in the differentiated state of the nerves, showing that the electrical stimulation has increased the rate of differentiation and/or degree of differentiation of PC-12s into a neural phenotype.[34,35] The average length of neurites per cell

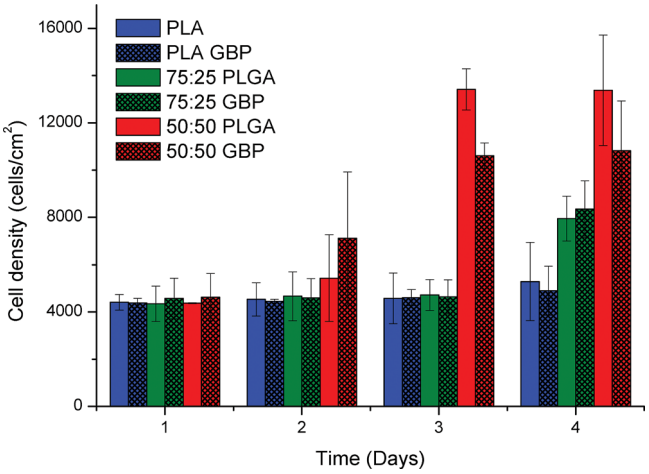

Figure 4. Proliferation of PC-12 cells on graphene-modified (GBP) and unmodified PLGA over 4 days. The cells were seeded at 3000 cells cm^{-2} on materials that were not coated with collagen or any other cell adhesion molecules and the cell densities were assessed at each time point using a Pico Green Assay to estimate the amount of DNA. The cell proliferation wasn't affected significantly by graphene coating, but was highly dependent on the underlying polymer, particularly at 48–72 h.

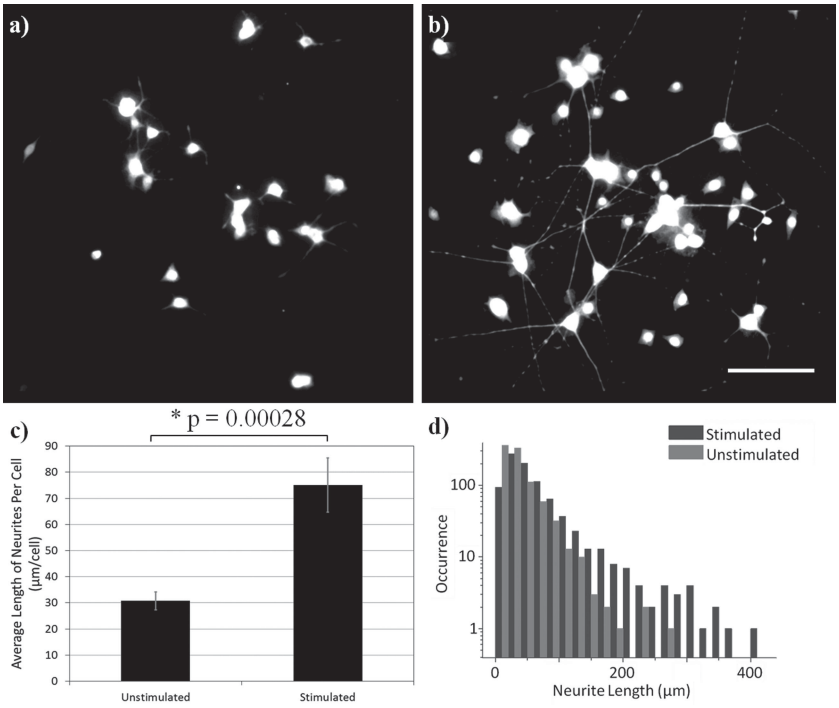

Figure 5. Differentiation of PC-12 cells on GBP structures and analysis of the image data. a) Fluorescence microscope images of PC-12 cells (immunostained to show βIII tubulin in cells) on graphene without and b) with electrical stimulation. c) Results of image analysis for neurite length performed over an 8 mm^2 area. The error bars show one standard deviation error of the mean, and the numbers describe the ANOVA statistics for comparison of stimulated and unstimulated cells, with * indicating a statistically significant difference. d) A histogram comparing the frequency of occurrence of neurite lengths in the stimulated and unstimulated populations. The scale bar represents 50 μm.

significantly increased (a 2.5-fold increase from 30 μm per cell to 75 μm per cell, $p = 0.00028$ by ANOVA) (Figure 5c), in addition to an increase in the number of longer neurites (greater than 100 μm) (Figure 5d). The increase in the number of longer neurites shows that a large proportion of the PC-12 cells are highly differentiated. This is supported by the image of the electrically stimulated cells in Figure 5b. However, the cell density and number of neurites per cell showed no difference with electrical stimulation (Figure S-3, Supporting Information), indicating that electrical stimulation increased the outgrowth of existing neurites, but did not induce the formation of new neurites. This result is very significant, as it demonstrates both the ability of the composite material to communicate with cells in order to modify their metabolism by providing electrical charge and also because it is the first literature report as far as we know of enhanced nerve cell differentiation using graphene electrodes. The successful electrical stimulation of PC-12 cells (as indicated by their enhanced differentiation); in combination with the ability to maintain the biocompatible properties (e.g., surface energy and mechanical) of the underlying polymer support show that the composite materials are sufficiently conductive to act as flexible electrodes capable of electrical communication with neural cells.

To confirm that the crystallinity of the graphene in the GBP structure was preserved after electrical stimulation, Raman mapping and spectral analysis were performed on the collagen-coated samples with fixed cells on the surface (**Figure 6**). The Raman spectra were segregated into three different data sets dependent on the 2D:G ratio (Figure 6a) and these data sets were overlaid with the optical image of each sample. The mapped data correlate to the presence of cells with a slight decrease in the 2D:G ratio of surrounding cells visible in the optical images. This decrease is attributed to light scattering from the fluids inside the cell in combination with the low signal intensity from the graphene. Over the bulk of the examined sample, taken through the cell adhesion collagen layer, the average 2D:G ratio was 2.0 ± 1.5 (mean ± standard deviation). This result confirms the structural stability of the graphene after electrical stimulation and the successful growth and differentiation of PC-12 nerve cells on GBP composite materials.

3. Conclusions

We have successfully demonstrated graphene-biopolymer structures useful for cell stimulation and studied the response of nerve cells on the composites. The development was made possible by the process of transferring CVD-grown bilayer graphene onto the non-conducting biocompatible underlying polymer to provide a conductive layer that does not interfere with the polymer properties relevant to biocompatibility and cell response to the material. Examining the interactions of these materials with PC-12 cells shows the addition of graphene onto the biopolymers did not change the

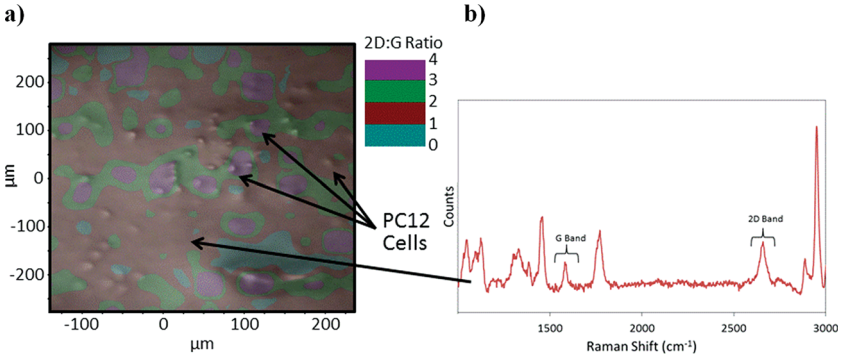

Figure 6. Raman spectra of GBP taken after electrical stimulation of PC-12 nerve cells, a) Raman map of 2D:G intensity ratio for 50:50 GPB composites after cell growth and electrical stimulation at 10× magnification; this maps demonstrateds an average 2D:G ratio of 1.7 ± 1.0; and b) typical Raman spectra show the presence of bilayer graphene on the surface and under the regions of PC-12 cells.

cell-substrate interactions and the overall cell densities were defined by the underlying biopolymer composite. The optimal polymer composition (50:50 PLGA) was used to prepare the GBP structures for the electrical stimulation studies. Electrical stimulation via the graphene layer enhanced the differentiation of neural cells, which for the first time demonstrates the efficacy of GBP structures for supplying charge to cells. These results show the ability of bilayer graphene to serve as a material to add surface electrical conductivity over a large area and over large morphological features of the polymer, suggesting this should be a suitable process to convert many polymers of widely varying properties and morphologies into conducting biomaterials. Most significantly, the process does not interfere with the biocompatible properties of the biomaterial. We have therefore demonstrated the ability of graphene sheets to 'mimic' the surface properties of the underlying polymer substrates and applicability of a graphene-biopolymer composite as an electrode to enhance nerve cell differentiation.

4. Experimental Section

Graphene Synthesis: Bilayer graphene was produced utilizing the decomposition of methane over 99.99% pure Cu foil (Sigma-Aldrich), using a method adapted from Wassei et al.[21] The graphene was grown at a maximum growth temperature of 985 °C and at a partial pressure of 1.1 mTorr.

Composite Preparation: 5% solutions of a. PLA (inherent viscosity midpoint 2.0 dl/g), b. 75:25 PLGA (inherent viscosity midpoint 0.7 dL g^{-1}), and c. 50:50 PLGA (inherent viscosity midpoint 0.4 dL g^{-1}) (Purasorb) were produced by dissolution in acetone. These solutions were drop-cast onto the produced Cu:graphene sheets such that the surface of the copper was fully coated. The copper film was etched using Copper Etchant (Sigma-Aldrich) followed by a 12 h soak in (20%) HCl and a 6-h wash with distilled water. Blank test samples were prepared by drop-casting of the equivalent polymer solutions onto Cu foils without graphene. The same etching procedure described above was applied to these blank samples.

Cell Proliferation: PC-12 cells (rat adrenal gland pheochromocytoma) in proliferation media (DMEM supplemented with 10% horse serum and 5% fetal bovine serum) were plated onto the GBP composite materials at 1000 cells per well in a 96 well plate. Cells were incubated at 37 °C and 5% CO_2 for 24, 48, 72, or 96 h, before the cell numbers in each well were determined using a Pico Green assay (Invitrogen). In short, the media was carefully removed from each well before the cells were lysed by two freeze/thaw cycles in 0.1% SDS/TE buffer, then 10 µL aliquots of each well were diluted with 90 µL TE buffer and added to 100 µL of Pico Green reagent diluted 1:200 in TE buffer, before the fluorescence of each well was read using a 485 nm excitation and 520 nm emission using a FLUOstar Omega (BMG Labtech). The fluorescence was converted to a cell number with reference to a standard curve of known cell densities.

Cell Differentiation: Differentiation of PC-12 cells into a neural phenotype was induced by plating cells in proliferation media overnight on 50:50 PLGA with or without a graphene coating, then changing to differentiation media (DMEM supplemented with (2%) horse serum with 50 ng mL^{-1} nerve growth factor). Electrical stimulation is known to increase the length of neurites extended by PC-12 cells undergoing differentiation, and so electrical stimulation of cells growing on graphene substrates was undertaken using a biphasic current waveform at 250 Hz, consisting of 100 µs pulses of ± 0.1 mA cm^{-2} with a 20 µs interphase gap, and a 3.88 ms rest period in each cycle. The counter electrode used in the 2 electrode setup was a platinum mesh, and the current was controlled using an 8-channel digital stimulator (DS8000, World Precision Instruments) with a stimulus isolator (A365, World Precision Instruments), with the voltages being recorded using an e-corder and Chart software (EDAQ Pty. Ltd). Cells were fixed using (3.7%) parafomaldehyde, and then immunostained with a mouse anti-βIII tubulin primary antibody, and an Alexa-594 donkey anti-mouse secondary antibody, as well as DAPI to stain the nuclei. Cells were imaged in a Leica AxioImager fluorescent microscope, and the images analysed by ImageJ, using the NeuronJ plug-in to quantify neurite lengths. Where neurites branched, the secondary branch was counted as a separate neurite, with the length counted from the branch point to the tip. The total neurite length for each field of view was quantified, as were the number of cells (by nuclei counting) and the data analysed using Microsoft Excel and Origin 8.

Characterization Techniques: Samples were analyzed by Raman spectroscopy using a Horiba Raman spectrometer equipped with a 632.8 HeNe laser and a 300 line mm^{-1} grating window. Raman maps were collected on this spectrometer with an automated stage with defined incremental steps. Ratio intensity maps were obtained by comparing the areas under the curve of the G and 2D bands using the LabSpec software. All GBP composite materials were characterized by Raman spectroscopy in 5 separate points with a local area map being attained for each film (not shown). Spectra were obtained using a 50× wide-angle lens unless otherwise stated.

Atomic force spectroscopy was performed using a JPK Nanowizard AFM in phosphate buffer saline solution (PBS). 20 nm diameter silicon nitride tips were used to apply a 40 nN force on the GBP samples for force spectra. Both force and height mapping analysis was performed in contact mode as this demonstrated the greatest tracking of the surface after experimental analysis.

Goniometer measurements were performed using a Data Physics Contact Angle system.

Supporting Information

Supporting Information is available from the Wiley Online Library or from the author.

Acknowledgements

The authors would like to thank W Zheng and S Naficy of the University of Wollongong and the Australian National Fabrication Facility (ANFF) for equipment use. The authors are grateful for financial support from the Australian Research Council's ARC Centre of Excellence for Electromaterials Science and Laureate Fellowship (GGW), FENA FCRP Center at UCLA (RBK) and the IMI program of the US National Science Foundation under Award No. DMR 0843934 (JKW).

Received: May 23, 2013
Revised: July 18, 2013
Published online: October 8, 2013

[1] G. G. Wallace, S. E. Moulton, R. M. I. Kapsa, M. J. Higgins, *Organic Bionics*, Wiley-VCH Verlag GmbH & Co. KGaA, Weinheim, Germany **2012**.
[2] G. G. Wallace, S. E. Moulton, G. M. Clark, *Science* **2009**, *324*, 185.
[3] E. W. Keefer, B.R. Botterman, M. I. Romero, A. F. Rossi, G. W. Gross, *Nat. Nanotechnol.* **2008**, *3*, 434.
[4] D.-H. Kim, R. Ghaffari, N. Lu, J. A. Rogers, *Ann. Rev. Biomed. Eng.* **2012**, *14*, 113.
[5] A. K. Geim, K. S. Novoselov, *Nat. Mater.* **2007**, *6*, 183.
[6] B. Matthias, *Surface Sci. Rep.* **2012**, *67*, 83.
[7] H. J. Park, J. Meyer, S. Roth, V. Skákalová, *Carbon* **2010**, *48*, 1088.
[8] S. Bhaviripudi, X. Jia, M. S. Dresselhaus, J. Kong, *Nano Lett.* **2010**, *10*, 4128.

[9] L. Liu, H. Zhou, R. Cheng, Y. Chen, Y.-C. Lin, Y. Qu, J. Bai, I. A. Ivanov, G. Liu, Y. Huang, X. Duan, *J. Mater. Chem.* **2012**, *22*, 1498.
[10] B. Hu, H. Ago,Y. Ito, K. Kawahara, M. Tsuji, E. Magome, K. Sumitani, N. Mizuta, K.-I. Ikeda, S. Mizuno, *Carbon* **2012**, *50*, 57.
[11] A. K. Geim, *Science* **2009**, *324*, 1530.
[12] X. Li, W. Cai, J. An, S. Kim, J. Nah, D. Yang, R. Piner, A. Velamakanni, I. Jung, E. Tutuc, S. K. Banerjee, L. Colombo, R. S. Ruof, *Science* **2009**, *324*, 1312.
[13] H. I. Rasool, E. B. Song, M. J. Allen, J. K. Wassei, R. B. Kaner, K. L. Wang, B. H. Weiller, J. K. Gimzewski, *Nano Lett.* **2010**, *11*, 251.
[14] N. J. Coville, S. D. Mhlanga, E. N. Nxumalo, A. Shaikje, *S. Afr. J. Sci.* **2011**, *107*, 1.
[15] L. Brown, R. Hovden, P. Huang, M. Wojcik, D. A. Muller, J. Park, *Nano Lett.* **2012**, *12*, 1609.
[16] E. V. Castro, K. S. Novoselov, S. V. Morozov, N. M. R. Peres, J. M. B. L. dos Santos, J. Nilsson, F. Guinea, A. K. Geim, A. H. C. Neto, *Phys. Rev. Lett.* **2007**, *99*, 216802.
[17] C. H. Lui, Z. Li, K. F. Mak, E. Cappelluti, T. F. Heinz, *Nat. Phys.* **2011**, *7*, 944.
[18] C. Chen, P. H. Lin, J.-M. Lu, C. Marin-Muller, H. Wang, X. Wang, Q. Yao, *Exp. Rev. Mol. Diagn.* **2009**, *9*, 325.
[19] G. Deniz, *Turk. J. Chemistry* **1999**, *23*, 153.
[20] L. Lu, C. A. Garcia, A. G. Mikos, *J. Biomed. Mater. Res.* **1999**, *46*, 236.
[21] A. P. Balgude, X. Yu, A. Szymanski, R. V. Bellamkonda, *Biomaterials* **2001**, *22*, 1077.
[22] Q. H. Wang, Z. Jin, K. K. Kim, A. J. Hilmer, G. L. C. Paulus, C.-J. Shih, M.-H. Ham, J. D. Sanchez-Yamagishi, K. Watanabe, T. Taniguchi, J. Kong, P. Jarillo-Herrero, M. S. Strano, *Nat. Chem.* **2012**, *4*, 724.
[23] J. K. Wassei, M. Mecklenburg,J. A. Torres, J. D. Fowler, B. C. Regan, R. B. Kaner, B. H. Weiller, *Small* **2012**, *8*, 1415.
[24] A. C. Ferrari, J. C. Meyer, V. Scardaci, C. Casiraghi, M. Lazzeri, F. Mauri, S. Piscanec, D. Jiang, K. S. Novoselov, S. Roth, A. K. Geim, *Phys. Rev. Lett.* **2006**, *97*, 187401.
[25] L. M. Malard, J. Nilsson, D. C. Elias, J. C. Brant, F. Plentz, E. S. Alves, A. H. Castro Neto, M. A. Pimenta, *Phys. Rev. B* **2007**, *76*, 201401.
[26] D. Graf, F. Molitor, Ensslin, C. Stampfer, A. Jungen, C. Hierold, L. Wirtz, *Nano Lett.* **2007**, *7*, 238.
[27] M. S. Dresselhaus, G. Dresselhaus, R. Saito, A. Jorio, *Phys. Rep.* **2005**, *409*, 47.
[28] M. S. Dresselhaus, A. Jorio, A. G. Souza Filho, G. Dresselhaus, R. Saito, *Phys. B: Condensed Matter* **2002**, *323*, 15.
[29] A. L. Mohana Reddy, N. Rajalakshmi, S. Ramaprabhu, *Carbon* **2008**, *46*, 2.
[30] E. Frackowiak, F. Béguin, *Carbon* **2001**, *39*, 937.
[31] C. Largeot, C. Portet, J. Chmiola, P.-L. Taberna, Y. Gogotsi, P. Simon, *J. Am. Chem. Soc.* **2008**, *130*, 2730.
[32] S. Shiraishi, H. Kurihara, K. Okabe, D. Hulicova, A. Oya, *Electrochem. Commun.* **2002**, *4*, 593.
[33] N. H. Lee, K. G. Weinstock, E. F. Kirkness, Kirkness, J. A. Earle-Hughes, R. A. Fuldner, S. Marmaros, A. Glodek, J. D. Gocayne, M. D. Adams, A. R. Kerlavage, *Proc. Natl. Acad. Sci. U. S. A.* **1995**, *92*, 8303.
[34] C. E. Schmidt, V. R. Shastri, J. P. Vacanti, R. Langer, *Proc. Natl. Acad. Sci. U. S. A.* **1997**, *94*, 8948.
[35] X. Liu, K. J. Gilmore, S. E. Moulton, G. G. Wallace, *J. Neural Eng.* **2009**, *6*, 065002.